

# COHERENT TIME REVERSAL SUB-ARRAY PROCESSING FOR MICROWAVE BREAST IMAGING

Foroohar Foroozan<sup>\*</sup>, Nazanin HosseinKhah<sup>\*\*</sup>, and Raviraj Adve<sup>†</sup>

<sup>\*</sup>Analog Devices, Canada, <sup>\*\*</sup>Department of Medical Biophysics, University of Toronto, <sup>†</sup>Department of ECE, University of Toronto

## ABSTRACT

This paper develops a new beamforming method using focused frequency time reversal (FFTR) matrices as well as the time reversal-based Multiple Signal Classification (MUSIC) algorithm to focus spatially on the location of possible tumor for microwaves-based breast cancer detection. A key feature of the proposed method is that there is no need for prior knowledge of the constitutive properties of the breast tissue for breast clutter suppression; sliding sub-aperture data processing is used to focus on tumor location. Results from our electromagnetic finite difference time domain (FDTD) simulations demonstrate the accuracy in estimating both the tumor location as well as in suppressing the breast clutter using time reversal.

**Index Terms**— Time Reversal, SVD, Microwave Imaging, Tumor Localization.

## 1. INTRODUCTION

Research on the applications of microwaves in medical diagnostics has been ongoing for more than 20 years. Results point toward substantial benefits in breast-cancer screening, breast-cancer treatment monitoring, bone-disease treatment monitoring as well as brain imaging [1]. Yet, to this day, microwave imaging has not entered clinical practice. A similar scenario arises in the nondestructive testing of materials and the nondestructive evaluation for structural integrity. What prevents this technology from realizing its potential? From an engineering viewpoint, one major problem is the insufficient sensitivity of the microwave equipment, i.e., its ability to detect very weak deviations in the signals. This is a critical factor that determines the sensitivity and the specificity of a diagnostics procedure. From an imaging and signal processing point of view, the main challenge for accurate breast tumor localization using microwaves lies in the lack of precise knowledge of constitutive properties of the breast tissue, as well as of the skin layer and chest wall morphology [2].

The time reversal (TR) method utilizes the reciprocity of wave propagation in a time-invariant medium to localize a target with high resolution [3]. The focusing quality in the time-reversal method is decided by the size of the effective aperture of transmitter-receiver array. This effective aperture includes the physical size of the array and the effect of the environment [4]. A complicated background such as breast tissue creates a multipath effect and can significantly increase the effective aperture size. Indeed, TR harnesses multipath propagation to enhance focusing resolution beyond the classical diffraction limit known as super-resolution which is attractive for many applications such as radar [5, 6], and breast microwave imaging [7–9]. TR-based imaging methods use the eigenstructure of the TR matrix to image the targets.

Generally, a singular value decomposition (SVD) of the TR matrix is required for each frequency bin and for each *space-space* TR-matrix [10, 11]. At each frequency, the singular vectors have an arbitrary and frequency-dependent phase. In case of DORT [3], these

arbitrary phases make the eigenvectors in the time domain incoherent and a pre-processing step is needed to apply coherent signals in the back propagation phase [12]. In TR-MUSIC [13], only the magnitude of the inner products are combined along the bandwidth and these arbitrary phases cancel out, therefore, the problem of incoherency does not exist for non-noisy data. However, due to the random phase structure induced by noise, the super-resolution property of TR-MUSIC disappears. A modified version of TR-MUSIC, Phase Coherent MUSIC (PC-MUSIC) [14] uses a re-formulation of TR-MUSIC which retains the phase information but also applies averaging of the pseudospectrums in frequency to cancel out the random phase degradation of the TR-MUSIC.

In order to reduce the computational complexity of incoherent TR-MUSIC as well as solving the phase ambiguity of the PC-MUSIC in a noisy microwave breast environment, in this paper, we use focused frequency TR-MUSIC (FFTR-MUSIC) [4], where we use TR-MUSIC in conjunction with TR-based frequency focusing matrices. In FFTR-MUSIC, the SVD is applied into a focused frequency TR matrix by finding unitary focusing matrices [15–17]. A second contribution of this paper is TR clutter suppression before using the coherent FFTR-MUSIC imaging method. The TR MUSIC-based methods require the number of elements in the antenna array to be greater than the total number of scattering elements (tumor and clutter) in the breast tissue which is not obviously possible. In contrast to the other TR-based imaging methods [18], our TR clutter suppression algorithm does not depend on background suppression of the clutter; rather, it suppresses the clutter using a sliding window of sub-aperture matrices to extract localized scattering information of a given breast scenario. This approach was originally proposed for ground-penetrating radar applications [19].

It is important to emphasize that the tumor data TR matrix contains both the direct reflections between the target and the receive array, and secondary reflections between the scatterers, target, and receiver array coming from multiple paths. The clutter background subtraction suppresses the clutter reflections and *not* the secondary scattering between the target, scatterers, and receiver. Therefore, to extract the TR data matrix for tumor in the presence of the clutter combined with the target returns, we use a method based on spatially sliding windows and synthesizing SVD distributions corresponding to localized scattering information. When SVD is applied to different subsections of the TR data matrix, the singular values and corresponding vectors will be combined to synthesize clutter signals that correspond to different scattering regions. We confirm the accuracy of our proposed imaging method using the electromagnetic finite difference time domain (FDTD) [20] simulations to detect the presence of a tumor within an MRI based breast model and contrast it with conventional Multiple-Input Multiple-output (MIMO) radar imaging methods.

## 2. SYSTEM MODEL

In this section, we introduce the observation models representing the forward and TR probing steps for the localization algorithm

proposed later in the paper. A known complex bandpass signal  $f_i(t) \exp(j\omega_c t)$  ( $\omega_c$  denoting the angular carrier frequency), transmitted by element  $i$  located at  $\mathbf{x}_i$  (for  $1 \leq i \leq N$ ) of an antenna array, is backscattered by the target (tumour) with unknown spatial location  $\mathbf{r}_t$ . After down conversion to baseband, the observations recorded by element  $j$  of the array located at  $\mathbf{x}_j$  in frequency domain is modeled as a multiplication of the transmitted signal with the background Green's functions through  $L$  paths and can be written as

$$R_{ij}(\omega) = \sum_{l=1}^L [X_{ijl} G_0(|\mathbf{r}_t - \mathbf{x}_i|_l, \omega) G_0(|\mathbf{x}_j - \mathbf{r}_t|_l, \omega) F_i(\omega)] + R_{ij}^c(\omega) F_i(\omega) + N_{ij}(\omega), \quad (1)$$

where  $F_i(\omega)$  is the Fourier transform of  $f_i(t)$ , and  $X_{ijl}$  represents both the attenuation factor for multipath  $l$  connecting receiving element  $j$  to transmitting element  $i$  and the reflection coefficient of the target. Notations  $R_{ij}^c$ , and  $N_{ij}(\omega)$  are, respectively, the frequency domain down-converted components of the clutter and noise. A dispersive, lossy homogeneous medium with uniform conductivity  $\sigma(\omega)$  is considered for the background Green's function [11], as

$$G_0(\mathbf{r}_l, \omega) \approx \frac{\exp(-jk\mathbf{r}_l - \sigma(\omega)\frac{\eta}{2}\mathbf{r}_l)}{\sqrt{\mathbf{r}_l}}. \quad (2)$$

Note that the wavenumber  $k = \omega\sqrt{\mu\epsilon}$  and  $\eta = \sqrt{\mu/\epsilon}$  with  $\epsilon$  and  $\mu$  being the permittivity and the permeability of the medium, respectively.

## 2.1. Conventional MIMO Radar for Breast Imaging

The conventional MIMO radar approach comprises of the following steps.

1. **Conventional Probing:** Assuming all transmitted signals be the same, i.e.,  $F(\omega)$ , in the matrix form, Eq. (1) is given as

$$\mathbf{R}(\omega) = \underbrace{\sum_{l=1}^L X_l \mathbf{K}_t^l(\omega) F(\omega)}_{\mathbf{R}_t(\omega)} + \underbrace{\mathbf{K}_c(\omega) F(\omega) + \mathbf{N}(\omega)}_{\mathbf{R}_z(\omega)} \quad (3)$$

where  $\mathbf{K}_t^l(\omega)$  is the transmit-receive response matrix of the tumor from path  $l$  for  $1 \leq l \leq L$  and  $\mathbf{K}_c(\omega)$  is the clutter response and the coefficients  $X_{ijl} = X_l$ . In terms of the target channel response  $\mathbf{R}_t(\omega)$  is the target response while  $\mathbf{R}_z(\omega)$  contains both the clutter response  $\mathbf{K}_c(\omega)F(\omega)$  and noise component  $\mathbf{N}(\omega)$ .

2. **Conventional Clutter Suppression:** In modeling  $\mathbf{K}_c(\omega)$ , we follow the approach presented in [21, 22], where the clutter is characterized in the spatial and spectral domains as a multivariate complex Gaussian random process. The clutter return  $\mathbf{R}_{r_c}(\omega) = \mathbf{K}_c(\omega)F(\omega)$  changes randomly over time and when multipath scattering is rich, can be represented as a random process, whose statistics are modeled as a multivariate complex Gaussian vector with zero mean and covariance of  $\mathbf{R}_{r_c}(\omega)$  [22]. With the noise component  $\mathbf{N}(\omega)$  assumed complex Gaussian, the covariance of the clutter-noise component  $\mathbf{R}_z$  is expressed as  $\mathbf{R}_{r_z} = \mathbf{R}_{r_c} + \sigma_n^2 \mathbf{I}_{N^2}$ . Noting that the clutter-noise covariance matrix  $\mathbf{R}_{r_z}$  is a positive definite matrix, a whitening filter is used to convert the clutter-noise

component to white noise. If the  $L$ -path target responses are summed in  $\mathbf{K}_t(\omega)$ , then the response matrix  $\tilde{\mathbf{R}}(\omega)$  is given by

$$\tilde{\mathbf{R}}(\omega) = \underbrace{\mathbf{R}_{r_z}^{-\frac{1}{2}} \mathbf{K}_t(\omega) F(\omega)}_{\tilde{\mathbf{R}}_t(\omega)} + \underbrace{\mathbf{R}_{r_z}^{-\frac{1}{2}} \mathbf{R}_z(\omega)}_{\tilde{\mathbf{R}}_z(\omega)}, \quad (4)$$

with the whitened clutter-noise term  $\tilde{\mathbf{R}}_z(\omega) \sim \mathcal{CN}(0, \mathbf{I}_{N^2})$ .

## 2.2. TR-MIMO Radar for breast Imaging

Recall that the TR framework time reverses the observations made during the forward probing stage and re-transmits them as probing signals during the TR probing step. In addition to Steps 1-2 outlined in Section 2.1 for the conventional MIMO radar, the TR-MIMO localization includes the following steps.

3. **TR Probing:** The whitened backscatters  $\tilde{\mathbf{R}}(\omega)$  from Eq. (4) are time-reversed, energy normalized, and are used to probe the medium a second time. Following the approach used to derive Eq. (3) in the forward probing step, the TR response matrix is given by

$$\mathbf{P}(\omega) = g \sum_{l'=1}^L X_{l'} \mathbf{K}_t^{l'}(\omega) \tilde{\mathbf{R}}^*(\omega) + \mathbf{K}_c(\omega) \tilde{\mathbf{R}}^*(\omega) + \mathbf{W}(\omega), \quad (5)$$

where  $\mathbf{W}(\omega)$  is the observation noise in the TR step. Substituting Eq. (3) in Eq. (5) gives

$$\begin{aligned} \mathbf{P}(\omega) = & g \sum_{l'=1}^L \sum_{l=1}^L X_l X_{l'} \mathbf{K}_t^{l'}(\omega) \mathbf{R}_{r_z}^{-1/2*} \mathbf{K}_t^{*l}(\omega) F^*(\omega) \quad (6) \\ & + \underbrace{g \sum_{l=1}^L X_l \mathbf{K}_c(\omega) \mathbf{R}_{r_z}^{-1/2*} \mathbf{K}_t^{*l}(\omega) F^*(\omega)}_{\mathbf{P}_c(\omega)} \\ & + \underbrace{g \sum_{l=1}^L X_l \mathbf{K}_t^l(\omega) \tilde{\mathbf{R}}_z^*(\omega) + g \mathbf{K}_c(\omega) \tilde{\mathbf{R}}_z^*(\omega) + \mathbf{W}(\omega)}_{\mathbf{P}_z(\omega)}. \end{aligned}$$

Eq. (6) decomposes the TR backscatter observation into three components: target backscatter, clutter returns and noise component. In [23], we proved that if the number of paths is large, as in the case for breast imaging [8], the target return double summation will be reduced to a single summation for same paths in forward and TR steps. Also, the accumulated noise component  $\mathbf{P}_z(\omega)$  can be approximated as white noise if the original noise in the conventional probing is white. Please refer to Appendices A and B in [23] for further details. Simplifying (6) using the above mentioned results, the TR observations become

$$\begin{aligned} \mathbf{P}(\omega) = & g \sum_{l=1}^L |X_l|^2 \mathbf{K}_t^l(\omega) \mathbf{R}_{r_z}^{-1/2*} \mathbf{K}_t^{*l}(\omega) F^*(\omega) \quad (7) \\ & + \mathbf{P}_c(\omega) + \mathbf{P}_z(\omega) \end{aligned}$$

Noting that the clutter returns in (6) is mixed with the target returns  $\mathbf{K}_t^{*l}(\omega)$ , simple background subtraction will not work in this situation. Next section explains a sub-array processing approach for clutter suppression in the TR-MIMO setup.

4. **TR Clutter Suppression:** The idea here is to use a sub-aperture of length  $M$  of the antenna array and study the SVD of each sub-aperture and the correlations to the neighboring sub-arrays. For example, the strongest singular value (and the corresponding vector) corresponds to the surface reflection from the skin [19]. Using sub-arrays instead of the full matrix allows us to extract more localized information about the target and clutter. We develop a spatially sliding window of length  $M$  and use this window for SVD calculations of the sub-arrays as follows.

$$\mathbf{P}_i^{\text{sub}}(\omega) \mathbf{v}_{i,m}^{\text{sub}}(\omega) = \lambda_{i,m}^{\text{sub}} \mathbf{u}_{i,m}^{\text{sub}}(\omega), \quad (8)$$

where  $\mathbf{P}_i^{\text{sub}}(\omega)$  denotes the TR matrix response of the  $i$ th sub-aperture and  $\mathbf{v}_{i,m}^{\text{sub}}(\omega)$ ,  $\mathbf{u}_{i,m}^{\text{sub}}(\omega)$ ,  $\lambda_{i,m}^{\text{sub}}$  are respectively, the  $m$ th right and left singular vectors and singular values of the sub-array  $i$ , ( $i = 1, \dots, N - M + 1$ ,  $M \leq N - i + 1$ ,  $1 \leq m \leq M$ ). Using weighted singular vector distributions, the clutter can be modeled as [19]

$$\mathbf{P}_c(\omega) = \sum_{m=1}^P \lambda_{i,m}^{\text{sub}} \mathbf{u}_{i,m}^{\text{sub}}(\omega). \quad (9)$$

The number  $P$  of singular vectors in (9) is defined by taking correlation coefficients between the neighboring sub-arrays to be greater than a threshold  $\tau$ . Then, the tumor response  $\mathbf{P}_t(\omega)$  after clutter subtraction is given as

$$\mathbf{P}_t(\omega) = \mathbf{P}(\omega) - \mathbf{P}_c(\omega). \quad (10)$$

### 3. COHERENT FFTR-MUSIC IMAGING

For imaging, we apply a coherent method using the concept of focusing matrices originally proposed in [15, 17] in conjunction with the TR-MUSIC. This method involves focusing matrices to transform the time reversal operator at different frequency bins onto a single reference frequency and a coherent focused time reversal operator is achieved. The reference frequency is assumed to be  $\omega_0$  and the unitary focusing matrices [15] for  $Q$  frequency bins ( $\omega_q$  for  $0 \leq q \leq (Q - 1)$ ) are to be found. These unitary matrices  $\mathbf{B}(\omega_q)$  minimize the difference between  $\mathbf{P}_t(\omega_0)$  and the transformed TR matrix at frequency  $\omega_q$  with the following minimization problem.

$$\begin{aligned} \min_{\mathbf{B}(\omega_q)} \|\mathbf{P}_t(\omega_0) - \mathbf{B}(\omega_q) \mathbf{P}_t(\omega_q)\|_F \\ \text{subject to } \mathbf{B}^H(\omega_q) \mathbf{B}(\omega_q) = \mathbf{I}, \end{aligned} \quad (11)$$

where  $\|\cdot\|_F$  denotes the Frobenius matrix norm. Applying SVD on the TR matrix  $\mathbf{P}_t(\omega_q)$ , it has been shown in [15] that the solution to the problem (11) is given by

$$\mathbf{B}(\omega_q) = \mathbf{V}(\omega_q) \mathbf{U}^H(\omega_q), \quad (12)$$

where  $\mathbf{V}(\omega_q)$  and  $\mathbf{U}(\omega_q)$  are the right and left eigenvalues of the TR matrix  $\mathbf{P}_t(\omega_q)$ . Then, the coherently focused TR operator is the weighted average of the transformed matrix of TR with unitary matrix  $\mathbf{B}(\omega_q)$  as follows

$$\tilde{\mathbf{P}}_t(\omega_0) = \sum_{q=0}^{(Q-1)} \beta_q \mathbf{B}(\omega_q) \mathbf{P}_t(\omega_q) \mathbf{B}^H(\omega_q), \quad (13)$$

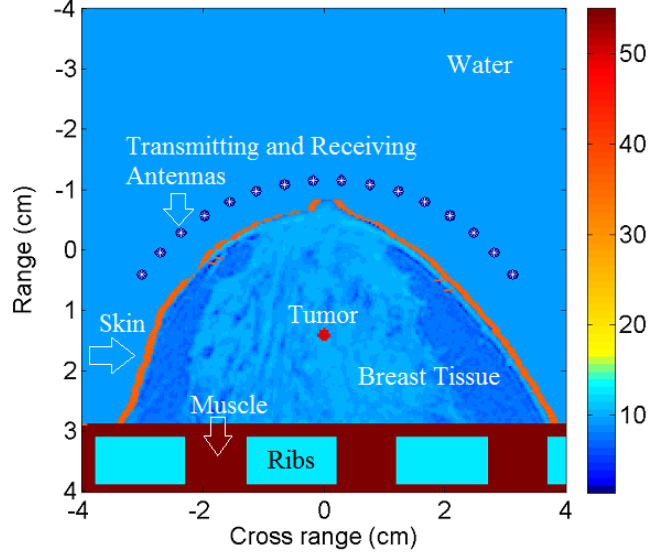


**Fig. 1:** Permittivity of the numerical domain comprised of transmitting and receiving antennas, water, breast skin, breast tissue, tumor, ribs and muscle between ribs.

Component in FDTD domain	Permittivity ( $\epsilon$ ) $\times 8.854^{-12}$ farad/meter	Conductivity ( $\sigma$ ) Siemens/meter
Water	9	0
Skin	36	4
Tumor	50	4
Breast Tissue	Derived from the MRI image	0.4
Ribs	11.6	4
Muscle	50	8

**Table 1:** Electromagnetic parameters and values.

where  $\beta_q$  is the  $q$ th weight proportional to the SNR of the this frequency bin. In summary, we first use the TR matrix to focus on frequency and then by using the focused TR matrix, we apply the TR-MUSIC to focus spatially on the scatterers. The advantage with this approach is that only the Green's function at the focused frequency is needed for image formation. It is worth noting that for incoherent TR-MUSIC and PC-MUSIC, the array steering vector should be computed for each frequency bin over the entire grid. The final step will be to form the pseudospectrum of FFTR-MUSIC as follows.

$$A(\omega_0, \mathbf{r}) = \frac{\mathbf{g}^H(\omega_0, \mathbf{r}) \mathbf{U}_{\text{Sig}}(\omega_0) \mathbf{U}_{\text{Sig}}^H(\omega_0) \mathbf{g}^*(\omega_0, \mathbf{r})}{\|\mathbf{g}(\omega_0, \mathbf{r})\|^2}, \quad (14)$$

where  $\mathbf{U}_{\text{Sig}}(\omega_0)$  is the signal subspace matrix at the focused frequency resulted from the SVD of  $\tilde{\mathbf{P}}_t(\omega_0)$  and  $\mathbf{g}(\omega_0, \mathbf{r}) = [G(|\mathbf{r} - \mathbf{x}_1|, \omega_0), \dots, G(|\mathbf{r} - \mathbf{x}_N|, \omega_0)]^T$ . Finally, the FFTR-MUSIC image is given by  $I(\mathbf{r}) = (1 - A(\omega_0, \mathbf{r}))^{-1}$ .

### 4. EXPERIMENTAL STUDY USING FDTD SIMULATIONS

In this study, a numerical analysis using electromagnetic finite difference time domain (FDTD) was performed in order to detect the presence of a tumor within an MRI-based breast model. Maxwell

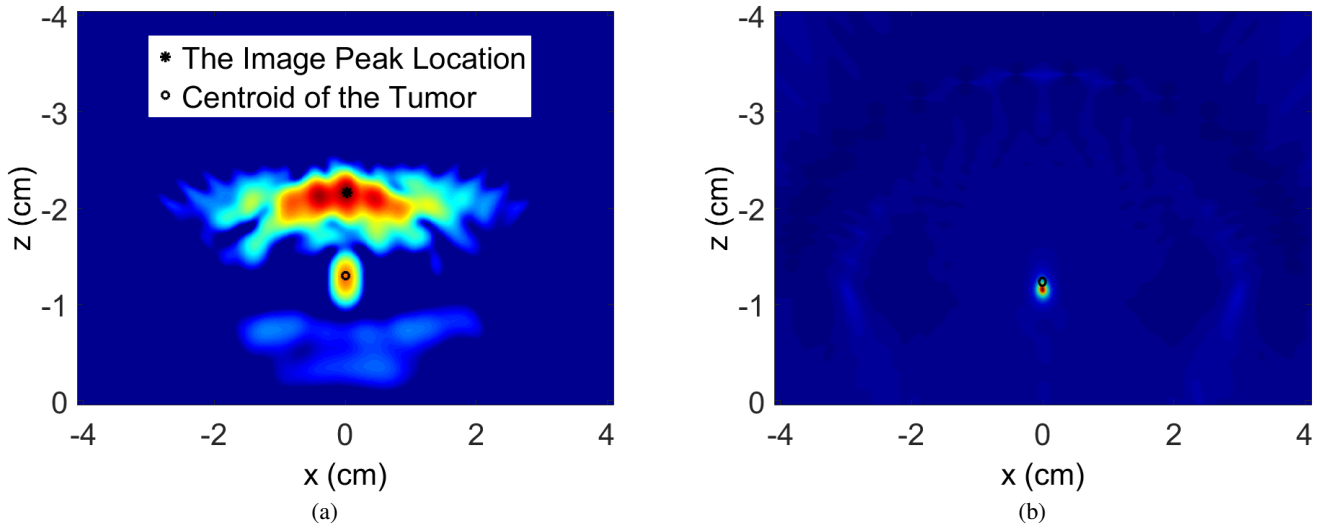


**Fig. 2:** MIMO radar imaging to detect the tumor location: (a) Conventional MIMO radar where the clutter is subtracted from the complete FDTD results with tumor. Symbol “o” represents the centroid of the tumor and \* represent the peak of the image; and (b) Coherent FFTR-MUSIC with the TR clutter suppression method.

equations were solved and based on the permittivity ( $\epsilon$ ) and conductivity ( $\sigma$ ) inputs of the model, signals were calculated at the antenna locations. Four perfectly matched boundary layers (PML), which are absorbing boundaries, were chosen to avoid reflections from the edges of the modeling grid. FDTD simulations were performed using MATLAB with a modified version of codes generated by Irving and Knight [20]. The overall electromagnetic domain had an  $8 \times 8$  cm geometry size. For numerically stable FDTD simulations, a temporal step of 0.4 ps was chosen. In order to avoid numerical dispersion in the FDTD results, the spatial spacing of  $\Delta x$  and  $\Delta z = 0.1$  mm were chosen in both the axial and lateral directions.

**Geometry:** In this study, a geometry comprising transmitting and receiving antennas, water, breast skin, breast tissue, tumor, ribs and muscle between ribs was simulated. The breast was assumed to be immersed in a lossless liquid. To simulate the breast tissue, a magnetic resonance image of a healthy breast was used as shown in Fig. 1. A logarithm of the breast tissue image was calculated and the results were scaled so that the mean relative permittivity to vacuum was 9 [2]. There was a 13.4% variability in permittivity values. The conductivity values of the breast tissue were set to  $\sigma = 0.4$  Siemens/meter. The breast boundaries were extracted and while preserving the boundary shape, a layer of the breast skin was added manually to the model (Fig. 1). The skin was given a 1-mm-thickness [24] with relative permittivity of 36 and conductivity of 4 [25]. As the chest wall was not shown in Fig. 1, the ribs and muscles in between the ribs were manually added to the geometry with appropriate electromagnetic properties [25], [26], [27]. As shown in Fig. 1, the ribs were 1.5 cm in width and at a 1 cm spacing apart [28].

A 1-mm tumor in radius located 1.5 cm from the chest wall was manually added to the simulation geometry (Fig. 1). The relative permittivity and conductivity of the tumor tissue were set to 50, and 4 S/m respectively [29]. Table 1 summarizes the electromagnetic parameters chosen for the simulations. A 16-element circular transmitting and receiving antenna arrays were placed 0.7 cm away from the breast. The antennas were 0.5 cm apart from each other. The data was acquired in a multi-static fashion, i.e., signals are transmit-

ted from each array elements, one antenna at a time, and recorded by all the antennas. A Gaussian pulse modulated with a 9 GHz carrier frequency ( $f_c$ ) was used as the probing signal. The following equation shows the probing signal used in this study:

$$f(t) = (1/\sqrt{2\pi t_1}) \exp(-1/2(t/t_1)^2) \sin(2\pi f_c t), \quad (15)$$

where the pulse width,  $t_1$ , was 0.05 ns.

**Beamforming:** As a result of the FDTD simulations, the total signals sent by each antenna and received by the other 16 were stored in a  $16 \times 16$  matrix. In another set of FDTD simulations in which tumor is not available, we have the clutter response. In order to exclude the antenna coupling, strong skin scattering as well as clutter, we subtracted the complete FDTD results with tumor from the clutter response for conventional imaging. Fig. 2(a) presents the result of the tumor detected using conventional MIMO observations  $\mathbf{R}(\omega)$  in comparison with the actual tumor location. It is important to note that a large scattering from the breast skin was observed in this figure which distorts the tumor location from its original position. Fig. 2(b), however shows the result of the TR backscatters  $\hat{\mathbf{P}}_t(\omega_0)$  to form the FFTR-MUSIC pseudospectrum given in Eq. (14). As shown in this image, the location of the tumor is close to the original tumor location and the skin, ribs and other clutter are almost removed. Sub-aperture window length of  $M = 4$  with %50 overlap is selected. The number  $p$  in Eq. (9) is selected as 3 with correlation threshold greater than 0.85 between the neighboring signals.

## 5. CONCLUSIONS

We conducted numerical FDTD simulations of the proposed TR beamforming scheme. Our imaging results demonstrate that the FFTR-MUSIC imager combined with the sliding sub-aperture data processing for clutter suppression achieves better accuracy, higher robustness to clutter, and increased resolution than the conventional direct subtraction MIMO imager.

## 6. REFERENCES

- [1] N. K. Nikolova, "Microwave biomedical imaging," *Wiley Encyclopedia of Electrical and Electronics Engineering*, 2014.
- [2] A. E. Fouda and F. L. Teixeira, "Ultra-wideband microwave imaging of breast cancer tumors via Bayesian inverse scattering," *Journal of Applied Physics*, vol. 115, no. 6, p. 064701, Feb. 2014.
- [3] C. Prada and J. Thomas, "Experimental subwavelength localization of scatterers by decomposition of the time reversal operator interpreted as a covariance matrix," *Journal of the Acoustical Society of America*, vol. 114, pp. 235–243, 2003.
- [4] F. Foroozan and P. Sadeghi, "Super-resolution ultrawideband ultrasound imaging using focused frequency time reversal music," in *2015 IEEE ICASSP*, April 2015, pp. 887–891.
- [5] F. Foroozan and A. Asif, "Time reversal based active array source localization," *IEEE Trans. on Signal Processing*, vol. 59, no. 6, pp. 2655–2668, June 2011.
- [6] F. Foroozan, A. Asif, Y. Jin, and J. Moura, "Direction finding algorithms for time reversal MIMO radars," *IEEE SSP*, pp. 433–437, 2011.
- [7] P. Kosmas and C. M. Rappaport, "Time reversal with the FDTD method for microwave breast cancer detection," *IEEE Transactions on Microwave Theory and Techniques*, vol. 53, no. 7, pp. 2317–2323, 2005.
- [8] J. Yuanwei, J. Yi, and J. M. F. Moura, "Time reversal beamforming for microwave breast cancer detection," in *Proceedings of IEEE International Conference on Image Processing (ICIP)*, vol. 5, pp. V–13–V–16, 16 2007–Oct. 19 2007.
- [9] Y. Jin, J. M. F. Moura, J. Yi, M. Wahl, H. Zhu, and Q. He, "Breast cancer detection by time reversal imaging," *IEEE International Symposium on Biomedical Imaging: From Nano to Macro, (ISBI)*, pp. 816–819, May 2008.
- [10] M. Yavuz and F. Teixeira, "Frequency dispersion compensation in time reversal techniques for UWB electromagnetic waves," *IEEE Geoscience and Remote Sensing Letters*, vol. 2, no. 2, pp. 233–237, April 2005.
- [11] —, "A numerical study of time-reversed UWB electromagnetic waves in continuous random media," *IEEE Antennas and Wireless Propagation Letters*, vol. 4, pp. 43–46, 2005.
- [12] —, "Full time-domain DORT for ultrawideband electromagnetic fields in dispersive, random inhomogeneous media," *IEEE Transactions on Antennas and Propagation*, vol. 54, no. 8, pp. 2305–2315, Aug. 2006.
- [13] F. K. Gruber, E. A. Marengo, and A. J. Devaney, "Time-reversal imaging with multiple signal classification considering multiple scattering between the targets," *Journal of the Acoustical Society of America*, vol. 115, no. 6, pp. 3042–3047, 2004.
- [14] E. G. Asgedom, L.-J. Gelius, A. Austeng, S. Holm, and M. Tygel, "Time-reversal multiple signal classification in case of noise: A phase-coherent approach," *The Journal of the Acoustical Society of America*, vol. 130, no. 4, pp. 2024–2034, 2011.
- [15] H. Hung and M. Kaveh, "Focussing matrices for coherent signal-subspace processing," *IEEE Transactions on Acoustics, Speech and Signal Processing*, vol. 36, no. 8, pp. 1272–1281, Aug 1988.
- [16] H. Wang and M. Kaveh, "Coherent signal-subspace processing for the detection and estimation of angles of arrival of multiple wide-band sources," *IEEE Transactions on Acoustics, Speech and Signal Processing*, vol. 33, no. 4, pp. 823–831, Aug 1985.
- [17] Z. Wang, J. Li, and R. Wu, "Time-delay- and time-reversal-based robust Capon beamformers for ultrasound imaging," *IEEE Transactions on Medical Imaging*, vol. 24, no. 10, pp. 1308–1322, Oct. 2005.
- [18] J. M. F. Moura and J. Yuanwei, "Time reversal imaging by adaptive interference canceling," *IEEE Transactions on Signal Processing*, vol. 56, no. 1, pp. 233–247, Jan. 2008.
- [19] M. E. Yavuz, A. E. Fouda, and F. L. Teixeira, "GPR signal enhancement using sliding-window space-frequency matrices," *Progress In Electromagnetics Research*, vol. 145, pp. 1–10, 2014.
- [20] J. Irving and R. Knight, "Numerical modeling of ground-penetrating radar in 2-D using MATLAB," *Computers & Geosciences*, vol. 32, no. 9, pp. 1247–1258, Nov. 2006.
- [21] Y. Jin, N. O'Donoghue, and J. Moura, "Time reversal adaptive waveform in MIMO radar," in *Proc. 2010 International Conference on Electromagnetics in Advanced Applications (ICEAA '10)*, Sydney, September 2010.
- [22] H. L. van Trees, *Detection, Estimation, and Modulation Theory: Part III, Radar-Sonar Signal Processing and Gaussian Signals in Noise*. New York, USA: Wiley-Interscience, 2001.
- [23] F. Foroozan, A. Asif, and Y. Jin, "Cramer-Rao bounds for time reversal mimo radars with multipath," *IEEE Transactions on Aerospace and Electronic Systems*, vol. 52, no. 1, pp. 137–154, February 2016.
- [24] T. L. Pope, M. E. Read, T. Medsker, A. J. Buschi, and A. N. Brenbridge, "Breast skin thickness: normal range and causes of thickening shown on film-screen mammography," *Journal of the Canadian Association of Radiologists*, vol. 35, no. 4, pp. 365–8, Dec. 1984.
- [25] S. Gabriel, R. W. Lau, and C. Gabriel, "The dielectric properties of biological tissues: II. Measurements in the frequency range 10 Hz to 20 GHz," *Physics in Medicine and Biology*, vol. 41, no. 11, pp. 2251–2269, Nov. 1996.
- [26] P. C. Pedersen, C. C. Johnson, C. H. Durney, and D. G. Bragg, "Microwave reflection and transmission measurements for pulmonary diagnosis and monitoring," *IEEE transactions on bio-medical engineering*, vol. 25, no. 1, pp. 40–8, Jan. 1978.
- [27] S. Gabriel, R. Lau, and C. Gabriel, "The dielectric properties of biological tissues: Iii. parametric models for the dielectric spectrum of tissues," *Physics in medicine and biology*, vol. 41, no. 11, p. 2271, 1996.
- [28] Y.-S. Kim, M. J. Park, H. Rhim, M. W. Lee, and H. K. Lim, "Sonographic analysis of the intercostal spaces for the application of high-intensity focused ultrasound therapy to the liver," *AJR. American journal of roentgenology*, vol. 203, no. 1, pp. 201–8, Jul. 2014.
- [29] S. C. Hagness, A. Taflove, and J. E. Bridges, "Two-dimensional FDTD analysis of a pulsed microwave confocal system for breast cancer detection: fixed-focus and antenna-array sensors," *IEEE transactions on bio-medical engineering*, vol. 45, no. 12, pp. 1470–9, Dec. 1998.